

Continual Unsupervised Out-of-Distribution Detection

Lars Doorenbos[✉], Raphael Sznitman[✉], and Pablo Márquez-Neila[✉]

University of Bern, Bern, Switzerland

{lars.doorenbos, raphael.sznitman, pablo.marquez}@unibe.ch

Abstract. Deep learning models excel when the data distribution during training aligns with testing data. Yet, their performance diminishes when faced with out-of-distribution (OOD) samples, leading to great interest in the field of OOD detection. Current approaches typically assume that OOD samples originate from an unconcentrated distribution complementary to the training distribution. While this assumption is appropriate in the traditional unsupervised OOD (U-OOD) setting, it proves inadequate when considering the place of deployment of the underlying deep learning model. To better reflect this real-world scenario, we introduce the novel setting of continual U-OOD detection. To tackle this new setting, we propose a method that starts from a U-OOD detector, which is agnostic to the OOD distribution, and slowly updates during deployment to account for the actual OOD distribution. Our method uses a new U-OOD scoring function that combines the Mahalanobis distance with a nearest-neighbor approach. Furthermore, we design a confidence-scaled few-shot OOD detector that outperforms previous methods. We show our method greatly improves upon strong baselines from related fields.

Keywords: Out-of-distribution detection · Continual learning

1 Introduction

Deep learning (DL) models fundamentally rely on the premise that the data distribution during training is congruent with that of the testing data. This assumption, when valid, enables these models to excel across a multitude of domains. However, this assumption often fails in real-world situations beyond the confines of controlled academic settings, primarily due to the emergence of unexpected samples, such as those stemming from issues with image acquisition. For these out-of-distribution (OOD) samples, the performance of DL models cannot be guaranteed, nor can they be readily identified. As a result, the dependability of DL models in applications where safety is paramount remains uncertain.

These shortcomings have sparked great interest in the field of OOD detection [17, 52]. OOD detectors are tasked with identifying and removing any sample that the underlying DL model can not reliably process, thereby increasing overall safety. Within the field, a natural distinction can be made between supervised

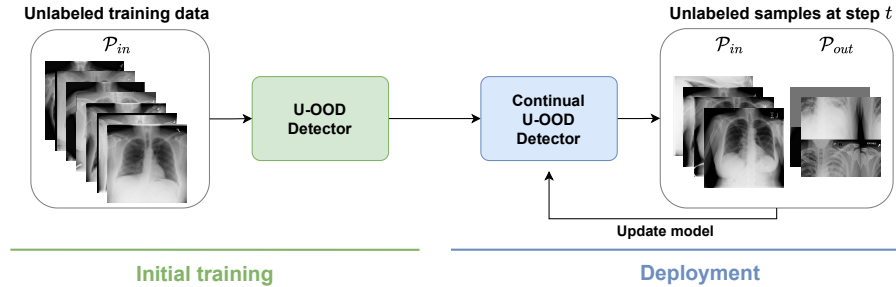


Fig. 1: The continual unsupervised out-of-distribution detection setting. In the first step, a U-OOD detector is trained using only unlabeled in-distribution data. Subsequently, during deployment, the OOD detector encounters real samples from both the in-distribution and out-distribution. Without knowing their categorization, these samples are integrated into the continual U-OOD detector, enhancing its ability to capture the actual OOD distribution accurately.

and unsupervised OOD detection. Supervised OOD detectors use either a labeled training dataset or explicit OOD samples to model the training distribution. In contrast, unsupervised OOD (U-OOD) detection assumes neither access to training labels nor OOD samples, leading to a more generally applicable albeit more challenging setting.

The same assumption that underpins closely related fields such as anomaly detection is used in current U-OOD works: normal samples are concentrated, whereas OOD samples are not [46, 48]. This reduces the problem of U-OOD to finding the level sets of the training data distribution and setting a threshold to define OOD samples. However, this assumption fails to consider the underlying motivation of OOD detection, that is, improving the reliability of downstream models. As U-OOD detectors cannot rely on training labels for context [1], we argue they must infer this from their deployment setting. In turn, the deployment context fully determines a *concentrated* OOD distribution.

To illustrate this, consider a U-OOD detector trained on a dataset of chest X-rays and intended for deployment in conjunction with a certain X-ray scanner. Within this context, the likelihood of encountering faulty images from scanner mishandling is magnitudes higher than encountering an image from a telescope or an image of the ocean. Furthermore, the exact composition of the OOD distribution depends entirely on external factors such as the scanner type and user proficiency. As a result, U-OOD works that synthesize anomalies (e.g., [45]) to simulate the OOD distribution are unable to capture this. Instead, an approach where an initial U-OOD detector, agnostic to the OOD distribution, is gradually updated during deployment to consider the actual OOD distribution is needed in practice (see Fig. 1).

Yet, current U-OOD research has mainly neglected this important consideration. Most closely related to this topic are the fields of OOD detection with in-the-wild data [8, 23] and OOD test-time adaptation [10, 54]. The former as-

sumes access to a large set of unlabeled data consisting of both *in-distribution* (ID) and OOD samples, whereas the latter uses the entire unlabeled test set to update a model. In both cases, hundreds of OOD samples are used to update their respective models. Consequently, this is often unrealistic, considering that OOD samples are scarce in real-world settings.

Instead, we focus here on improving detection with only a few OOD samples and tackle the setting where this process is iterative: detect OOD samples, update the OOD detector, and subsequently repeat the procedure with a refined model several times. Consequently, evaluating U-OOD detectors should extend beyond a single instance and consider their effectiveness *over time*. To do this, we propose the setting of continual U-OOD detection, where detectors are evaluated over multiple timesteps. In the first timestep, a standard U-OOD detector is trained using unlabeled in-distribution data only. For every subsequent timestep, the model is deployed to assess unlabeled test samples, including a limited number of out-of-distribution samples, which need to be incorporated into the model. We believe this setting most closely mimics that of the real world. As such, the main contributions of the present work are:

1. We introduce the problem of continual U-OOD detection, which closely matches the reality of model deployment. By doing so, we introduce new metrics and benchmarks to evaluate methods in this setting.
2. We propose a confidence-scaled few-shot OOD detector, which uses a U-OOD scoring function combining the Mahalanobis distance with a nearest-neighbor approach.
3. We propose a novel method for continual U-OOD detection that outperforms strong baselines from multiple related fields.

2 Related Work

The vast majority of OOD works fall into either supervised or unsupervised OOD. Supervised OOD methods assume access to a labeled training dataset [9, 17, 20, 22, 28, 29, 44, 49], while unsupervised methods learn the training distribution from a set of unlabeled samples only [2, 3, 7, 19, 25, 31, 32, 38–41, 47]. After training, these methods are evaluated on a test set once and the final performance is given. More closely related to the present work is the setting of OOD detection for continual classification [14]. However, our work focuses on continuous evaluation of (U-)OOD detection, which, to the best of our knowledge, has not been explored thus far. We describe related fields below, along with their differences with respect to continual U-OOD.

Test-time adaptation in OOD (TTA-OOD) is closely related to our work in that the entire unlabeled test set is used to update an OOD detector, and the performance is assessed after processing all samples. TTA-OOD works include AdaODD [10], which keeps a memory bank of features that is updated using confident pseudo-in and pseudo-OOD samples to score subsequent test samples. Another approach, ETLT [10], employs linear regression to predict the

output of an OOD detector. Similarly, [8, 16, 23, 56] assume a large set of unlabeled data consisting of in- and OOD samples is available after deployment.

Crucially, TTA-ODD works only consider the setting with thousands of test samples readily available rather than investigating the progression of OOD detectors over time. As a result, they differ from our setting in two important ways. First, assuming a large test set with many OOD samples is unrealistic due to their relative scarcity. Second, evaluating OOD detectors only after a large amount of data is collected rather than its evolution ignores the more realistic and challenging early stage of exposure to OOD samples. Additionally, all these methods require access to the original labeled training set.

Outlier exposure [18] uses a large auxiliary dataset of samples that can be considered outliers in conjunction with the training data to train an improved OOD detector. OE has been successfully applied to increase the performance of many OOD detectors [11, 18, 19, 36, 38, 42, 44], but its usefulness is limited when the OE distribution is far from the OOD distribution [39]. Related to our work, [30] find that a simple classification approach between in-distribution and OE data is effective for deep anomaly detection on images and note that by increasing the amount of OE data, an unsupervised approach should transition into a supervised approach. However, they do not investigate *how* to make this transition, nor do they use unlabeled test samples but rather confirmed OE outliers.

OOD with limited labels. Several fields deal with OOD detection in the presence of limited labels. For instance, few-shot OOD methods assume access to a small number of labeled OOD samples [11, 34, 47]. Other works consider the case where a handful of samples per class in the training set are available [6, 12]. In semi-supervised OOD, a small set of labeled anomalies is available next to a sizeable unlabeled set of normal data [16, 35, 43, 56]. Continual U-OOD can be seen as a sequence of few-shot OOD experiments with imperfect labels obtained from the previous model.

3 Continual U-OOD

The goal of U-OOD detection is to detect OOD samples and prevent them from being processed by a downstream model. In this setting, the training distribution of the downstream model is often called the *in distribution* \mathcal{P}_{in} , and the *out distribution* \mathcal{P}_{out} is assumed to be its *complement*. Given its large support, producing a set of OOD samples representative of \mathcal{P}_{out} for supervised classification of ID vs. OOD samples is intractable. Instead, U-OOD detection methods rely on in-distribution (ID) samples to train a detector $\sigma^{\text{in}}: \mathcal{X} \rightarrow \mathbb{R}$ that scores the *OOD-ness* of test samples at inference time. Moreover, the likelihood of observing a specific image from \mathcal{P}_{out} is not uniform once a downstream task is established and the model is deployed in a given environment. Instead, OOD samples detected during the operation of the deployed system, which depends on the downstream task and the deployment environment, are representative and constrain \mathcal{P}_{out} to the specific application. The goal of continual U-OOD is

to progressively enrich the detector σ^{in} with the observed OOD samples, thus adapting the detection model to the realities of the deployment environment.

More specifically, a continual U-OOD system builds a sequence of detectors $s_t(\mathbf{x}) : \mathcal{X} \mapsto \mathbb{R}$ for time steps $t \in \{0, 1, 2, \dots\}$. The sequence starts with the base U-OOD detector, $s_0 = \sigma^{\text{in}}$, and progressively adapts to the OOD samples observed after deployment. At each time t , the detector s_t is trained with the dataset of samples observed until the time step t , denoted by $\mathcal{D}_t = \mathcal{D}_t^{\text{train}} \cup \mathcal{D}_t^{\text{deploy}}$. The training dataset $\mathcal{D}_t^{\text{train}}$ contains the ID samples used to train both the downstream model and the base U-OOD detector σ^{in} , while the deployment dataset $\mathcal{D}_t^{\text{deploy}}$ contains ID and OOD samples observed during the operation of the deployed system until time t . We assume that $\mathcal{D}_0^{\text{deploy}} = \emptyset$.

Training detector s_t with \mathcal{D}_t is a supervised process, but not all elements in \mathcal{D}_t are labeled as ID or OOD. That is, elements of $\mathcal{D}_t^{\text{train}}$ are known to come from \mathcal{P}_{in} and are, therefore, ID samples. In contrast, the elements of $\mathcal{D}_t^{\text{deploy}}$ are samples of the *deployment distribution* $\mathcal{P}_{\text{deploy}}$ that, following [8, 23], can be modeled with the Huber contamination model [21],

$$\mathcal{P}_{\text{deploy}} = (1 - \pi)\mathcal{P}_{\text{in}} + \pi\mathcal{P}_{\text{out}}, \quad (1)$$

with OOD sample ratio π . Consequently, the nature of the elements in $\mathcal{D}_t^{\text{deploy}}$ is unknown. We leverage the sequential nature of the detectors and use s_{t-1} to pseudo-label the elements of $\mathcal{D}_t^{\text{deploy}}$ and train s_t with them. At each time t , the dataset \mathcal{D}_t can be split into two disjoint subsets $\mathcal{D}_t^{\text{in}}$ and $\mathcal{D}_t^{\text{out}}$ containing the samples labeled as ID and the samples labeled as OOD, respectively.

For simplicity and without loss of generality, we assume that the deployment dataset $\mathcal{D}_t^{\text{deploy}}$ grows K elements at each time step, whereby $|\mathcal{D}_t^{\text{deploy}}| = t \cdot K$. We will also omit the index t where not explicitly needed.

3.1 Model

The main challenge of OOD detection is the scarcity of representative OOD samples. In continual U-OOD detection, the expected number of OOD samples at time step t is $\pi \cdot t \cdot K$, which for a small t is too small to effectively train a binary classifier, preventing us from just using binary classifiers to model the detector s_t . As t increases, however, the feasibility of training a binary classifier improves. We, therefore, design our detection model s_t to behave as a few-shot learner s^- when t is close to 0 and to gradually transition towards a strong binary learner s^+ as t increases. Formally, we model the detector s_t as a convex combination of two learner modalities controlled by a mixing factor α_t ,

$$s_t(\mathbf{x}) = (1 - \alpha_t)s_t^-(\mathbf{x}) + \alpha_t s_t^+(\mathbf{x}). \quad (2)$$

The key difference between the learners s^- and s^+ relies on their inductive biases. The few-shot learner s^- is a low-variance/high-bias classifier with strong assumptions about in- and out-distributions. Its design is based on top of the U-OOD detector σ^{in} , as detailed below. In contrast, the strong learner s^+ is a

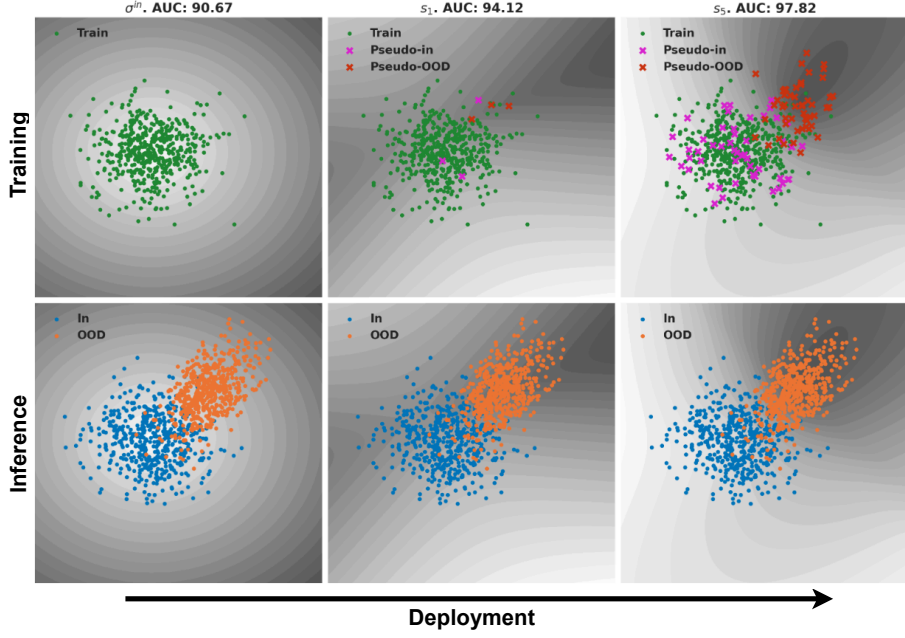


Fig. 2: Application of our method on toy data. A darker background indicates more OOD. In the first stage, we train our U-OOD base detector σ^{in} . During early deployment, our method relies heavily on the few-shot learner s^- , which can increase performance with a handful of pseudo-labeled test samples. Later on, given sufficient pseudo-labeled test samples providing information about \mathcal{P}_{out} , we put more weight on the binary classifier s^+ .

low-bias classifier, and its architecture can be chosen according to the nature of the input space \mathcal{X} (e.g., a CNN or a transformer architecture for image data), as our approach is agnostic to the internal specifics of s^+ . At each step t , both s_t^- and s_t^+ are trained independently with the dataset \mathcal{D}_t pseudo-labeled with s_{t-1} .

The factor $\alpha_t \in [0, 1]$ controls the transition between both models and is proportional to the number of OOD elements in \mathcal{D}_t ,

$$\alpha_t = \min(1, \beta \cdot |\mathcal{D}_t^{out}|), \quad (3)$$

where the factor β is a hyperparameter of our method.

The next sections describe our U-OOD detector σ and how it is used to define the few-shot learner s^- .

U-OOD detector: Our U-OOD detector combines elements from the Mahalanobis anomaly detector (MahaAD) [41], known for its robustness and speed [7], and from non-parametric nearest-neighbor scoring methods [2, 38, 49, 50]. As in MahaAD, given the collection of ID samples $\mathcal{D}^{in} = \{\mathbf{x}_i\}_{i=1}^N$, we fit a Gaussian

parameterized by the data mean μ and data covariance matrix Σ . To prevent numerical problems with near-singular covariance matrices in high-dimensional or low-data regimes, shrinkage is applied, resulting in the regularized covariance matrix,

$$\Sigma' = (1 - \nu)\Sigma + \nu \frac{\text{Tr}(\Sigma)}{d} \mathbf{I}_d, \quad (4)$$

where the shrinkage factor ν is found using the standard hyperparameter-free method of [27] and d is the data dimensionality. MahaAD uses the induced Mahalanobis distance $d_{\Sigma'}(\mathbf{x}, \mu)$ between the data mean μ and a test sample \mathbf{x} to estimate its OOD score. We instead use this distance to perform a k-NN search and score test samples with the average distance to their k nearest neighbors,

$$\sigma^{\text{in}}(\mathbf{x}) = \frac{1}{k} \sum_{\mathbf{x}' \in N_{\Sigma'}^k(\mathbf{x})} d_{\Sigma'}(\mathbf{x}, \mathbf{x}'), \quad (5)$$

where $N_{\Sigma'}^k(\mathbf{x})$ denotes the k -nearest neighbors of \mathbf{x} in the training data measured with the Mahalanobis distance induced by Σ' .

The detector σ^{in} defined in Eq. (5) is inappropriate for image samples, as the Mahalanobis distance is not a reliable measure of image similarity on high-dimensional spaces. Instead, when dealing with images, we first describe each image \mathbf{x}_i with a sequence of feature vectors $\{\mathbf{f}_\ell(\mathbf{x}_i)\}_{\ell=1}^L$, where \mathbf{f}_ℓ denotes the result of applying global average pooling on the feature map of the ℓ -th layer of a pre-trained convolutional neural network \mathbf{f} . We then use the descriptors of the training images to build a collection of layer-wise detectors $\{\sigma_\ell^{\text{in}}\}_{\ell=1}^L$. In particular, the detector σ_ℓ^{in} at layer ℓ applies the Eq. (5) with the covariance matrix Σ'_ℓ computed from the collection of features $\{\mathbf{f}_\ell(\mathbf{x}_i)\}_{i=1}^N$. The final OOD score for a test image \mathbf{x} is the sum of the scores over all layers,

$$\sigma^{\text{in}}(\mathbf{x}) = \sum_{\ell=1}^L \sigma_\ell^{\text{in}}(\mathbf{f}_\ell(\mathbf{x})). \quad (6)$$

Few-shot learner s^- : Our few-shot learner extends the OOD detector σ^{in} trained with \mathcal{D}^{in} by incorporating a twin detector σ^{out} trained with \mathcal{D}^{out} . The OOD score of the few-shot learner is computed as the difference between both detectors,

$$s^-(\mathbf{x}) = \sigma^{\text{in}}(\mathbf{x}) - \lambda \sigma^{\text{out}}(\mathbf{x}), \quad (7)$$

where the factor λ controls the influence of σ^{out} in the final score. The value of λ depends on the confidence levels of the detectors, which, in turn, rely on the contents in \mathcal{D}^{in} and \mathcal{D}^{out} . For instance, a small number of samples in \mathcal{D}^{out} will result in high uncertainty in the estimations of σ^{out} , which should be compensated with a small λ , and vice versa.

To measure the confidence of a detector σ trained with the dataset \mathcal{D} , we assess its variability under bootstrapping. More specifically, we produce M bootstrap samples $\{\mathcal{D}^{(m)}\}_{m=1}^M$ of N elements randomly sampled from \mathcal{D} with replacement, and compute the covariance matrices $\Sigma^{(m)}$ for each sample $\mathcal{D}^{(m)}$. The

uncertainty of the detector is measured as the variability of the bootstrapped covariance matrices,

$$U(\mathcal{D}) = \frac{1}{Md^2} \sum_{m=1}^M \left\| \boldsymbol{\Sigma}^{(m)} - \bar{\boldsymbol{\Sigma}} \right\|_F^2, \quad (8)$$

where $\bar{\boldsymbol{\Sigma}} = \frac{1}{M} \sum_m \boldsymbol{\Sigma}^{(m)}$. The factor λ is then computed as the ratio between the uncertainties of the detectors,

$$\lambda = \min \left(1, \gamma \frac{U(\mathcal{D}^{\text{in}})}{U(\mathcal{D}^{\text{out}})} \right), \quad (9)$$

where $\gamma > 0$ is a hyperparameter of our method. If no OOD samples are available, $U(\mathcal{D}^{\text{out}}) \rightarrow \infty$ and $\lambda = 0$, thus making the few-shot learner s^- equivalent to the base OOD detector σ^{in} .

When working with image data, we proceed layer by layer, as previously discussed for the OOD detector. In particular, we build a few-shot learner s_ℓ^- per each layer ℓ of the feature extractor \mathbf{f} , and the final score is the sum of the layer-wise scores,

$$s^-(\mathbf{x}) = \sum_{\ell=1}^L s_\ell^-(\mathbf{f}_\ell(\mathbf{x})). \quad (10)$$

4 Experiments

In the following section, we describe our experimental setup to evaluate continual U-OOD. To assess the performance of our approach, seven baselines are evaluated on three proposed benchmarks. In addition, we also perform an ablation study to identify contributing aspects of our method and compare our setting to outlier exposure, i.e., having access to a large dataset of auxiliary outliers from the unconstrained \mathcal{P}_{out} .

4.1 Experimental set-up

Baselines: We compare our method to seven baselines that comprise the top-performing methods from related fields: AdaODD [54], ETLT [10], and SAL [8] from OOD test-time adaptation, BCE from outlier exposure [30], the Mahalanobis difference (MDiff) [47] from few-shot OOD, and HSC [30] from semi-supervised OOD. Furthermore, we include MahaAD [41] as a U-OOD baseline. All methods use the same ImageNet pre-trained backbone.

To ensure fairness, our method and all baselines use a grid search procedure to set hyperparameters. We measure the performance of each method on the CIFAR10 experiment `Plane:Rest` and select the highest-performing configuration over the grid. The ranges considered for each hyperparameter in the grid search are given in the supplementary material.

Datasets: We introduce three continual U-OOD benchmarks on which we compare our method against the baselines under varying settings:

1. **Multi-class:** we adapt two common benchmarks with CIFAR10 and CIFAR100 [26] as the in-distribution [8, 23]. For both datasets, we run experiments with SVHN [33], resized LSUN [53], resized TinyImageNet [29], Places365 [55], and Describable Textures [4] as OOD. For LSUN and TinyImageNet, we use the fixed versions from [50]. Each experiment has $T = 5$ steps with $K = 100$ unlabeled samples and contamination $\pi = 0.1$.
2. **One-class:** continual versions of the ten quintessential one-class experiments on CIFAR10 [26], where one of the classes is the in-distribution and the other nine comprise the out-distribution [7, 38, 50]. Each experiment has $T = 10$, $K = 40$ and $\pi = 0.25$.
3. **High-resolution:** three experiments with high-resolution images selected from [7]. The first trains on healthy chest X-rays and uses pathological chest X-rays as OOD [51]. The second is **Real:Infograph** on DomainNet [37], which uses real images as in and infographs as OOD. The third has healthy retinal fundus photographs as the in-distribution, with the strongest level of diabetic retinopathy as OOD [13]. For all three cases, we set $T = 5$, $K = 50$, and $\pi = 0.2$.

There is no overlap between the test samples utilized for evaluating the quality of the methods and those belonging to $\mathcal{D}_t^{\text{deploy}}$.

Evaluation metrics: The two metrics commonly used to measure the performance of OOD methods are the false positive rate at 95% true positive rate (FPR@95) and the area under the receiver operating characteristic curve (AUC) [9, 29, 49]. In contrast with previous works, we are interested in measuring the quality of the OOD detector over time. As such, we propose two metrics that consider this aspect: the Area Under the FPR@95 curve (AUF) and the Area Under the AUC curve (AUA). These are computed by first evaluating the FPR@95 and AUC at every timestep and plotting the resulting FPR@95/AUC curves with respect to t . Then, the AUF and AUA are given by the area under the FPR@95 and AUC curves, respectively, normalized by the time elapsed.

Implementation details: Our pre-trained model \mathbf{f} is a ResNet-18 [15] pre-trained on ImageNet [5]. For s^- , we extract features from $L = 4$ layers at the end of every ResNet block and normalize the features of the final layer following [10, 39]. The binary classifier s^+ also uses a ResNet-18 architecture. It is trained with Adam [24] using a learning rate of 10^{-5} and a batch size of 256 for ten epochs on CIFAR10 and an equivalent number of iterations on the other datasets. We apply data augmentation in the form of random resized crops, color jitter, and horizontal flips and initialize the binary classifier with the weights from the previous timestep. At every step, the elements of $\mathcal{D}_t^{\text{deploy}}$ are re-labeled with the current model $s_t(\mathbf{x})$ using a threshold. The threshold is determined on the training data such that 95% is considered in-distribution. We

Table 1: Comparative evaluation on Multi-class. We report the mean of the AUF (\downarrow) and AUA (\uparrow) over five trials. **Bold** and underlined indicate best and second best, respectively. On average, our method obtains the best performance.

	SVHN		LSUN		ImgNet		Places		DTD		Mean	
	AUF	AUA										
<i>CIFAR10</i>												
SAL	91.4	63.3	93.2	52.6	91.6	55.6	82.7	62.1	92.2	53.6	89.9	56.0
HSC	94.6	53.4	86.4	61.8	80.0	64.8	33.2	90.5	87.5	60.7	76.3	66.2
ETLT	87.8	56.7	85.4	66.0	68.2	71.9	27.9	88.9	85.1	58.2	70.9	68.3
MahaAD	63.0	86.2	84.5	71.7	64.6	76.7	22.4	92.4	85.0	64.3	63.9	78.3
BCE	6.0	98.3	63.1	76.5	77.8	68.3	26.2	92.0	83.1	64.0	51.2	79.8
AdaODD	67.4	83.7	68.2	82.1	47.1	86.0	15.8	95.7	<u>70.7</u>	<u>79.0</u>	53.8	85.3
MDiff	1.3	99.7	<u>58.2</u>	<u>85.7</u>	61.3	78.8	<u>13.7</u>	<u>96.1</u>	75.0	72.9	41.9	<u>86.6</u>
ours	<u>3.0</u>	<u>99.2</u>	51.4	88.9	<u>53.4</u>	<u>83.7</u>	11.1	97.2	65.7	81.4	36.9	90.1
<i>CIFAR100</i>												
SAL	93.5	54.9	84.8	61.4	94.4	52.2	88.0	56.0	92.8	54.8	90.7	55.9
HSC	99.8	34.8	95.1	53.1	91.8	53.0	56.8	81.5	96.0	50.4	87.9	54.6
ETLT	98.8	35.6	98.2	50.0	90.7	58.0	47.3	79.8	96.6	44.8	86.3	53.6
MahaAD	96.8	62.1	97.0	56.0	85.3	63.5	40.2	84.3	95.8	49.7	83.0	63.1
BCE	<u>33.2</u>	<u>86.1</u>	85.7	63.9	92.2	53.9	56.2	77.8	92.6	56.2	72.0	67.6
AdaODD	93.8	55.7	93.0	61.6	78.0	73.4	37.3	87.5	<u>90.5</u>	<u>63.0</u>	78.5	68.2
MDiff	25.6	95.3	88.9	<u>72.1</u>	83.7	67.5	<u>32.5</u>	<u>89.0</u>	93.0	60.9	64.7	<u>77.0</u>
ours	55.8	85.3	<u>88.4</u>	74.4	<u>79.9</u>	<u>70.7</u>	28.3	91.6	89.7	66.6	<u>68.4</u>	77.7

standardize the scores of s^+ and s^- before combining them to ensure they have similar scales.

4.2 Results

Tab. 1 reports the results for **Multi-class**. Out of all methods, SAL, HSC, and ETLT are unable to outperform the unsupervised MahaAD baseline in any scenario. Unsurprisingly, we find the gradient-based filtering in SAL unable to detect OOD samples with the ImageNet pre-trained network. We also observe that the supervised classifier BCE is generally inconsistent; for instance, it achieves excellent results when SVHN is the OOD distribution but performs below average in the other cases. In contrast, AdaODD scores consistently high in all experiments except for SVHN but is, in turn, outclassed by MDiff. More broadly, our method is consistently among the top performers, reaching the best score for LSUN, Places, and DTD with both CIFAR10 and CIFAR100 as the in-distribution and scoring second-best in three out of the four remaining experiments.

In the **One-class** benchmark (Tab. 2), HSC also struggles, while ETLT consistently outperforms MahaAD, unlike on the **Multi-class** benchmark. AdaODD and MDiff again perform well, but which one is better between them depends on the experiment. Here, we also find our method to outperform all cases but

Table 2: Comparative evaluation on One-class. We report the mean of the AUF (↓) over five trials (AUA in supplementary). **Bold** and underlined indicate best and second best, respectively. Our method is the best overall.

	Plane	Car	Bird	Cat	Deer	Dog	Frog	Horse	Ship	Truck	Mean
SAL	82.9	46.6	85.2	80.0	78.5	78.8	64.7	78.4	63.5	40.4	69.9
HSC	64.2	57.1	86.6	81.6	71.9	79.3	53.3	61.2	48.9	52.1	65.6
ETLT	47.8	23.1	61.7	69.3	34.8	48.9	40.7	42.4	27.2	20.3	41.6
MahaAD	49.6	27.8	65.0	74.9	36.4	51.5	43.9	46.4	33.0	20.6	44.9
BCE	41.6	29	53.8	54	47.5	52	33.2	50	31	29.1	42.1
AdaODD	35.7	13.0	56.5	59.1	<u>26.9</u>	37.8	<u>25.1</u>	22.0	21.6	10.8	30.9
MDiff	28.3	18.6	<u>45.7</u>	<u>50.3</u>	31	<u>37.2</u>	25.9	31.6	<u>19.4</u>	15.6	<u>30.4</u>
ours	<u>29.5</u>	<u>14.0</u>	43.2	49.9	26.4	34.0	22.6	22.0	17.8	<u>12.5</u>	27.2

Table 3: Comparative evaluation on High-resolution. We report the mean of the AUF (↓) and AUA (↑) over five trials. **Bold** and underlined indicate best and second best, respectively. We obtain the best or second performance on all datasets.

	NIH		DN		DRD	
	AUF	AUA	AUF	AUA	AUF	AUA
SAL	89.5	56.8	90.5	54.9	66.0	74.4
HSC	66.0	<u>79.7</u>	79.6	70.2	80.7	71.9
ETLT	56.1	81.6	85.8	70.6	62.9	78.7
MahaAD	53.8	85.3	83.4	73.9	68.7	78.5
BCE	68.8	67.9	45.5	80.5	43.2	86.5
AdaODD	<u>46.8</u>	<u>87.0</u>	89.8	76.3	56.2	83.6
MDiff	49.7	82.4	28.6	<u>92.2</u>	55.0	84.6
ours	39.3	89.8	<u>36.3</u>	93.5	<u>53.9</u>	<u>85.1</u>

three, where it performs second-best. On **High-resolution**, Tab. 3 reports similar trends for our method ranking best or second in all six cases. Interestingly, BCE, which performs poorly on average across all three benchmarks, reaches the best performance on DRD.

The performance evolution for some of the best methods on the **Bird:Rest** and **Healthy:Pathological** experiments are shown in Fig. 3. All methods benefit from incorporating unlabeled samples, with the exception of AdaODD, whose optimal hyperparameters from the grid search assign low importance to the unlabeled data.

4.3 Ablations

We ablate our design choices by showing that (1) our OOD scoring function combining the Mahalanobis distance with k-nearest neighbors (MkNN) outperforms both kNN and MahaAD for U-OOD detection and (2) our few-shot learner s^-

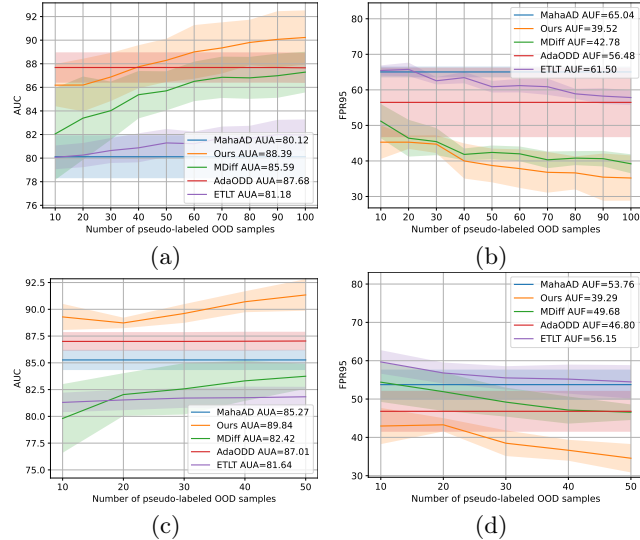


Fig. 3: Performance curves for top-performing methods. We show the AUC and FPR@95 curves for **Bird:Rest** in (a) and (b), and for **Healthy:Pathological** in (c) and (d). Our method achieves the best results and can improve results with a few unlabeled test samples.

outperforms unscaled scoring functions on few-shot OOD. To do so, we run experiments with our method on the standard one-class CIFAR10 benchmark. For few-shot OOD, we run experiments in the 5- and 10-shot settings. Here, n -shot refers to using n ground-truth OOD samples from the test set. For CIFAR10, this implies that the 5-shot setting will, by definition, not include an example of all OOD classes, as there are nine classes in the OOD distribution. Similarly, the 10-shot case will often not cover the whole class distribution due to the random selection of the 10 OOD samples.

We show the results for U-OOD in Tab. 4. MkNN outperforms the kNN scoring by 5.9 AUC and MahaAD by 1.6 AUC, showcasing its practical usefulness as MahaAD is one of the top-performing U-OOD detectors [7]. From Tab. 5, we find that equipping MDiff with our confidence scaling, which we label as (s_{Maha}^-) , improves the results by 6.5 AUC and 2 AUC in the 5- and 10-shot case, respectively. Furthermore, we improve the results by a further 0.6 and 0.8 AUC by using MkNN.

4.4 Continual U-OOD vs. Outlier Exposure

To illustrate the importance of continual U-OOD, we show how using a small number of unlabeled samples obtained iteratively during deployment is beneficial compared to the standard OE setting, which uses a large dataset of auxiliary outliers. For OE, we take 50'000 images from TinyImageNet as the outliers and

Table 4: Comparing U-OOD performance on CIFAR10. We report the AUC over one run as the methods are deterministic. **Bold** indicates the best method. MkNN is the best scoring function in all ten U-OOD experiments.

	Plane	Car	Bird	Cat	Deer	Dog	Frog	Horse	Ship	Truck	Average
kNN	80.0	75.5	86.3	79.6	82.7	82.4	87.7	76.5	82.4	84.3	81.7
MahaAD	86.2	78.0	89.3	88.7	85.6	80.8	92.1	79.5	90.0	90.0	86.0
MkNN (ours)	88.3	80.3	89.9	89.6	87.3	84.2	92.7	81.9	90.9	90.3	87.6

Table 5: Comparing few-shot OOD performance on CIFAR10. We report the mean AUC over five runs. **Bold** indicates the best method. Our few-shot detector s_{MkNN}^- is best overall.

	Plane	Car	Bird	Cat	Deer	Dog	Frog	Horse	Ship	Truck	Average
<i>5-shot</i>											
kNN	85.8	79.8	77.5	70.4	74.6	72.0	80.5	64.6	80.4	70.7	75.6
MDiff	90.2	92.1	80.0	75.5	83.0	82.6	89.7	76.1	88.9	89.1	84.7
s_{Maha}^- (ours)	91.7	94.4	84.7	83.3	92.2	90.5	92.4	92.4	94.1	96.4	91.2
s_{MkNN}^- (ours)	93.1	95.2	87.0	84.3	92.4	90.7	92.6	92.6	93.5	96.3	91.8
<i>10-shot</i>											
kNN	87.6	82.0	79.5	74.5	79.0	77.0	85.7	70.4	83.2	78.9	79.8
MDiff	92.8	94.5	84.1	80.7	90.6	86.6	93.9	88.4	93.3	93.9	89.9
s_{Maha}^- (ours)	92.5	94.8	85.7	84.2	92.8	90.9	93.5	92.5	95.2	96.7	91.9
s_{MkNN}^- (ours)	93.9	95.7	87.4	85.0	93.7	91.6	94.1	93.2	95.2	96.9	92.7

train a binary classifier between the in-distribution and out-distribution [30]. We compare this to the results obtained with our method using the continual U-OOD setting of the previous experiments.

Fig. 4 shows that even when pseudo-labeling $\mathcal{D}_t^{\text{deploy}}$ containing only 10 OOD samples, continual U-OOD is already far more effective than OE with 50'000 samples, with the gap widening as $|\mathcal{D}_t^{\text{deploy}}|$ increases. This is especially true when there is a mismatch between OE and OOD distributions, such as for the medical images in **Healthy:Pathological** (Fig. 4b).

4.5 Varying Contamination Ratios

We investigate the effectiveness of our proposed method compared to two baselines under varying contamination ratios π while keeping the number of OOD samples per step fixed at ten. We show results on CIFAR10:TinyImageNet and

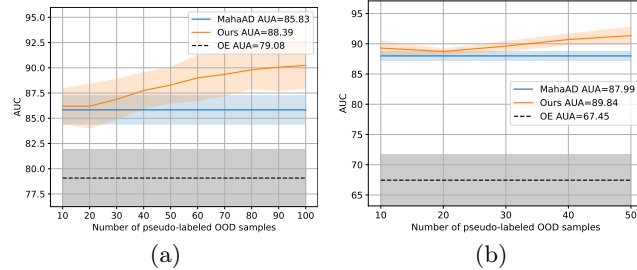


Fig. 4: Comparing continual U-OOD with Outlier Exposure. We show the AUA (\uparrow) for Bird:Rest in (a) and Healthy:Pathological in (b). Continual U-OOD is far more effective than OE, especially in the case of a mismatch between OE and OOD distributions.

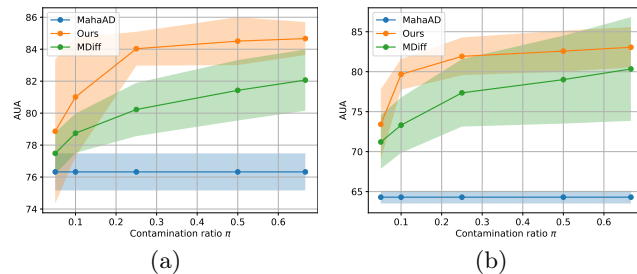


Fig. 5: Comparing methods under varying contamination ratios. We show the AUA per contamination ratio for CIFAR10:TinyImageNet in (a) and CIFAR10:DTD in (b). Our method outperforms the baselines at all contamination levels.

CIFAR10:DTD in Fig. 5. Our method achieves a better AUA for all contamination levels. As expected, the methods benefit from having a higher fraction of unlabeled OOD samples in the test set. Nonetheless, with a contamination ratio as low as 0.05 (i.e., $\mathcal{D}_t^{\text{deploy}}$ contains 200 unlabeled samples, of which only ten are OOD), we still outperform the unsupervised baseline by 2.5 AUA on CIFAR10:TinyImageNet and 9.1 AUA on CIFAR10:DTD.

5 Conclusion

In this work, we introduced the setting of continual U-OOD, which reflects the iterative process of real-world model deployment, along with new metrics and benchmarks for this task. Furthermore, we presented a novel method for continual U-OOD that pseudo-labels incoming samples and gradually transforms the base U-OOD detector into a binary classifier. In doing so, we additionally introduced a novel OOD scoring function that uses the Mahalanobis distance to compute a nearest-neighbors score and a few-shot OOD detector that takes into account the confidence of the distributions involved. Extensive experiments showed that our simple approach outperforms methods from several related fields.

References

1. Ahmed, F., Courville, A.: Detecting semantic anomalies. In: Proceedings of the AAAI Conference on Artificial Intelligence. vol. 34, pp. 3154–3162 (2020) [2](#)
2. Bergman, L., Cohen, N., Hoshen, Y.: Deep nearest neighbor anomaly detection. arXiv preprint arXiv:2002.10445 (2020) [3](#), [6](#)
3. Choi, H., Jang, E., Alemi, A.A.: Waic, but why? generative ensembles for robust anomaly detection. arXiv preprint arXiv:1810.01392 (2018) [3](#)
4. Cimpoi, M., Maji, S., Kokkinos, I., Mohamed, S., Vedaldi, A.: Describing textures in the wild. In: Proceedings of the IEEE conference on computer vision and pattern recognition. pp. 3606–3613 (2014) [9](#)
5. Deng, J., Dong, W., Socher, R., Li, L.J., Li, K., Fei-Fei, L.: Imagenet: A large-scale hierarchical image database. In: 2009 IEEE conference on computer vision and pattern recognition. pp. 248–255. Ieee (2009) [9](#)
6. Dong, J., Gao, Y., Zhou, H., Cen, J., Yao, Y., Yoon, S., Sun, P.D.: Towards few-shot out-of-distribution detection. arXiv preprint arXiv:2311.12076 (2023) [4](#)
7. Doorenbos, L., Sznitman, R., Márquez-Neila, P.: Data invariants to understand unsupervised out-of-distribution detection. In: European Conference on Computer Vision. pp. 133–150. Springer (2022) [3](#), [6](#), [9](#), [12](#)
8. Du, X., Fang, Z., Diakonikolas, I., Li, Y.: How does unlabeled data provably help out-of-distribution detection? International Conference on Learning Representations (2024) [2](#), [4](#), [5](#), [8](#), [9](#), [19](#)
9. Du, X., Wang, Z., Cai, M., Li, Y.: Vos: Learning what you don't know by virtual outlier synthesis. International Conference on Learning Representations (2022) [3](#), [9](#)
10. Fan, K., Wang, Y., Yu, Q., Li, D., Fu, Y.: A simple test-time method for out-of-distribution detection. arXiv preprint arXiv:2207.08210 (2022) [2](#), [3](#), [8](#), [9](#), [19](#)
11. Fort, S., Ren, J., Lakshminarayanan, B.: Exploring the limits of out-of-distribution detection. Advances in Neural Information Processing Systems **34**, 7068–7081 (2021) [4](#)
12. Gautam, C., Kane, A., Ramasamy, S., Sundaram, S.: Unsupervised out-of-distribution detection using few in-distribution samples. In: ICASSP 2023-2023 IEEE International Conference on Acoustics, Speech and Signal Processing (ICASSP). pp. 1–5. IEEE (2023) [4](#)
13. Graham, B.: Kaggle diabetic retinopathy detection competition report. University of Warwick **22** (2015) [9](#)
14. He, J., Zhu, F.: Out-of-distribution detection in unsupervised continual learning. In: Proceedings of the IEEE/CVF Conference on Computer Vision and Pattern Recognition. pp. 3850–3855 (2022) [3](#)
15. He, K., Zhang, X., Ren, S., Sun, J.: Identity mappings in deep residual networks. In: Computer Vision–ECCV 2016: 14th European Conference, Amsterdam, The Netherlands, October 11–14, 2016, Proceedings, Part IV 14. pp. 630–645. Springer (2016) [9](#)
16. He, R., Li, R., Han, Z., Yang, X., Yin, Y.: Topological structure learning for weakly-supervised out-of-distribution detection. In: Proceedings of the 31st ACM International Conference on Multimedia. pp. 4858–4866 (2023) [4](#)
17. Hendrycks, D., Gimpel, K.: A baseline for detecting misclassified and out-of-distribution examples in neural networks. International Conference on Learning Representations (2017) [1](#), [3](#)

18. Hendrycks, D., Mazeika, M., Dietterich, T.: Deep anomaly detection with outlier exposure. International Conference on Learning Representations (2019) 4
19. Hendrycks, D., Mazeika, M., Kadavath, S., Song, D.: Using self-supervised learning can improve model robustness and uncertainty. Advances in neural information processing systems **32** (2019) 3, 4
20. Hsu, Y.C., Shen, Y., Jin, H., Kira, Z.: Generalized odin: Detecting out-of-distribution image without learning from out-of-distribution data. In: Proceedings of the IEEE/CVF Conference on Computer Vision and Pattern Recognition. pp. 10951–10960 (2020) 3
21. Huber, P.J.: Robust estimation of a location parameter. In: Breakthroughs in statistics: Methodology and distribution, pp. 492–518. Springer (1992) 5
22. Kamoi, R., Kobayashi, K.: Why is the mahalanobis distance effective for anomaly detection? arXiv preprint arXiv:2003.00402 (2020) 3
23. Katz-Samuels, J., Nakhleh, J.B., Nowak, R., Li, Y.: Training ood detectors in their natural habitats. In: International Conference on Machine Learning. pp. 10848–10865. PMLR (2022) 2, 4, 5, 9
24. Kingma, D.P., Ba, J.: Adam: A method for stochastic optimization. International Conference on Learning Representations (2015) 9
25. Kirichenko, P., Izmailov, P., Wilson, A.G.: Why normalizing flows fail to detect out-of-distribution data. Advances in neural information processing systems **33**, 20578–20589 (2020) 3
26. Krizhevsky, A., Hinton, G., et al.: Learning multiple layers of features from tiny images (2009) 9
27. Ledoit, O., Wolf, M.: A well-conditioned estimator for large-dimensional covariance matrices. Journal of multivariate analysis **88**(2), 365–411 (2004) 7
28. Lee, K., Lee, K., Lee, H., Shin, J.: A simple unified framework for detecting out-of-distribution samples and adversarial attacks. Advances in neural information processing systems **31** (2018) 3
29. Liang, S., Li, Y., Srikant, R.: Enhancing the reliability of out-of-distribution image detection in neural networks. International Conference on Learning Representations (2018) 3, 9
30. Liznerski, P., Ruff, L., Vandermeulen, R.A., Franks, B.J., Müller, K.R., Kloft, M.: Exposing outlier exposure: What can be learned from few, one, and zero outlier images. Transactions on Machine Learning Research (2022) 4, 8, 13, 19
31. Márquez-Neila, P., Sznitman, R.: Image data validation for medical systems. In: Medical Image Computing and Computer Assisted Intervention–MICCAI 2019: 22nd International Conference, Shenzhen, China, October 13–17, 2019, Proceedings, Part IV 22. pp. 329–337. Springer (2019) 3
32. Nalisnick, E., Matsukawa, A., Teh, Y.W., Gorur, D., Lakshminarayanan, B.: Do deep generative models know what they don't know? International Conference on Learning Representations (2019) 3
33. Netzer, Y., Wang, T., Coates, A., Bissacco, A., Wu, B., Ng, A.Y.: Reading digits in natural images with unsupervised feature learning (2011) 9
34. Pang, G., Ding, C., Shen, C., Hengel, A.v.d.: Explainable deep few-shot anomaly detection with deviation networks. arXiv preprint arXiv:2108.00462 (2021) 4
35. Pang, G., Shen, C., Jin, H., van den Hengel, A.: Deep weakly-supervised anomaly detection. In: Proceedings of the 29th ACM SIGKDD Conference on Knowledge Discovery and Data Mining. pp. 1795–1807 (2023) 4
36. Papadopoulos, A.A., Rajati, M.R., Shaikh, N., Wang, J.: Outlier exposure with confidence control for out-of-distribution detection. Neurocomputing **441**, 138–150 (2021) 4

37. Peng, X., Bai, Q., Xia, X., Huang, Z., Saenko, K., Wang, B.: Moment matching for multi-source domain adaptation. In: Proceedings of the IEEE/CVF international conference on computer vision. pp. 1406–1415 (2019) [9](#)
38. Reiss, T., Cohen, N., Bergman, L., Hoshen, Y.: Panda: Adapting pretrained features for anomaly detection and segmentation. In: Proceedings of the IEEE/CVF Conference on Computer Vision and Pattern Recognition. pp. 2806–2814 (2021) [3, 4, 6, 9](#)
39. Reiss, T., Hoshen, Y.: Mean-shifted contrastive loss for anomaly detection. In: Proceedings of the AAAI Conference on Artificial Intelligence. vol. 37, pp. 2155–2162 (2023) [3, 4, 9](#)
40. Ren, J., Liu, P.J., Fertig, E., Snoek, J., Poplin, R., Depristo, M., Dillon, J., Lakshminarayanan, B.: Likelihood ratios for out-of-distribution detection. In: Advances in Neural Information Processing Systems. pp. 14707–14718 (2019) [3](#)
41. Rippel, O., Mertens, P., Merhof, D.: Modeling the distribution of normal data in pre-trained deep features for anomaly detection. In: 2020 25th International Conference on Pattern Recognition (ICPR). pp. 6726–6733. IEEE (2021) [3, 6, 8, 19](#)
42. Ruff, L., Vandermeulen, R.A., Franks, B.J., Müller, K.R., Kloft, M.: Rethinking assumptions in deep anomaly detection. ICML 2021 Workshop on Uncertainty and Robustness in Deep Learning (2021) [4](#)
43. Ruff, L., Vandermeulen, R.A., Görnitz, N., Binder, A., Müller, E., Müller, K.R., Kloft, M.: Deep semi-supervised anomaly detection. International Conference on Learning Representations (2020) [4](#)
44. Sastry, C.S., Oore, S.: Detecting out-of-distribution examples with gram matrices. In: International Conference on Machine Learning. pp. 8491–8501. PMLR (2020) [3, 4](#)
45. Schlüter, H.M., Tan, J., Hou, B., Kainz, B.: Natural synthetic anomalies for self-supervised anomaly detection and localization. In: European Conference on Computer Vision. pp. 474–489. Springer (2022) [2](#)
46. Schölkopf, B., Smola, A.J.: Learning with kernels: support vector machines, regularization, optimization, and beyond. MIT press (2002) [2](#)
47. Sehwag, V., Chiang, M., Mittal, P.: Ssd: A unified framework for self-supervised outlier detection. International Conference on Learning Representations (2021) [3, 4, 8, 20](#)
48. Steinwart, I., Hush, D., Scovel, C.: A classification framework for anomaly detection. Journal of Machine Learning Research **6**(2) (2005) [2](#)
49. Sun, Y., Ming, Y., Zhu, X., Li, Y.: Out-of-distribution detection with deep nearest neighbors. In: International Conference on Machine Learning. pp. 20827–20840. PMLR (2022) [3, 6, 9](#)
50. Tack, J., Mo, S., Jeong, J., Shin, J.: Csi: Novelty detection via contrastive learning on distributionally shifted instances. Advances in neural information processing systems **33**, 11839–11852 (2020) [6, 9](#)
51. Tang, Y.X., Tang, Y.B., Peng, Y., Yan, K., Bagheri, M., Redd, B.A., Brandon, C.J., Lu, Z., Han, M., Xiao, J., et al.: Automated abnormality classification of chest radiographs using deep convolutional neural networks. NPJ digital medicine **3**(1), 70 (2020) [9](#)
52. Yang, J., Zhou, K., Li, Y., Liu, Z.: Generalized out-of-distribution detection: A survey. arXiv preprint arXiv:2110.11334 (2021) [1](#)
53. Yu, F., Seff, A., Zhang, Y., Song, S., Funkhouser, T., Xiao, J.: Lsun: Construction of a large-scale image dataset using deep learning with humans in the loop. arXiv preprint arXiv:1506.03365 (2015) [9](#)

54. Zhang, Y., Wang, X., Zhou, T., Yuan, K., Zhang, Z., Wang, L., Jin, R., Tan, T.: Model-free test time adaptation for out-of-distribution detection. arXiv preprint arXiv:2311.16420 (2023) [2](#), [8](#), [19](#)
55. Zhou, B., Lapedriza, A., Khosla, A., Oliva, A., Torralba, A.: Places: A 10 million image database for scene recognition. IEEE transactions on pattern analysis and machine intelligence **40**(6), 1452–1464 (2017) [9](#)
56. Zhou, Z., Guo, L.Z., Cheng, Z., Li, Y.F., Pu, S.: Step: Out-of-distribution detection in the presence of limited in-distribution labeled data. Advances in Neural Information Processing Systems **34**, 29168–29180 (2021) [4](#)

A Supplementary Material

A.1 Baseline Details

We briefly describe all baselines and their hyperparameter ranges considered in the grid search. The ranges are based on the values found in each method’s original publication. To adapt them to the continual U-OOD setting, we apply the baselines sequentially, pseudo-labeling new samples with the model from the previous timestep. Further method-specific adaptations, if any, are detailed below. All methods use a ResNet18 pre-trained on ImageNet with images resized to 224×224 .

HSC [30] aims to obtain compact representations for ID samples while pushing features of anomalous samples further away. We search over the learning rate $lr \in [1e^{-4}, 1e^{-5}, 1e^{-6}]$, and pseudo-labeling threshold $\tau \in [80, 90, 95, 98]$. The threshold is a percentage such that $\tau\%$ of the training data is considered in-distribution. The best-performing configuration was $lr = 1e^{-6}, \tau = 80$.

ETLT [10] computes OOD scores for all available samples with a standard OOD detector, then fits linear regression to features extracted from a trained classifier to predict these scores. PCA is used to reduce the dimensionality of the feature vectors. We use MahaAD to compute the initial OOD scores to predict and swap the classifier for a pre-trained network. We search over the dimensionality $d \in [64, 128, 256, 512]$. The best-performing configuration was $d = 256$.

MahaAD [41] scores samples by summing the Mahalanobis distances to the training mean per layer. Used as a U-OOD baseline and comes without hyperparameters.

BCE [30] trains a binary classifier at every step and pseudo-labels samples with the resulting model. The exception is the first step, where we rely on MahaAD as the base detector. We search over the learning rate $lr \in [1e^{-4}, 1e^{-5}]$, OOD oversampling factor $oof \in [10, 50]$, and pseudo-labeling threshold $\tau \in [80, 90, 95]$. The best-performing configuration was $lr = 1e^{-5}, oof = 10, \tau = 90$.

SAL [8] finds candidate OOD samples based on their gradients with respect to the predicted label using a trained classifier, then trains a binary ID/OOD classifier together with the standard empirical risk minimization loss. We swap out the classifier for the pre-trained network and only train the binary classifier, as we do not have access to class labels. We search over the number of singular vectors $c \in [1, 2, 5, 10, 128, 256, 512]$ and use the same training settings as BCE. The best-performing configuration was $c = 512, lr = 1e^{-5}, oof = 10, \tau = 90$.

AdaODD [54] keeps a memory bank of normalized features extracted from a classifier. It scores samples with a kNN score. Confidently pseudo-labeled test samples are added to the memory bank. We swap the classifier for the pre-trained network. We search over the number of neighbors $k \in [2, 10, 50]$, selection margin $\gamma \in [1, 1.5, 2]$, and OOD scaling factor $\kappa \in [2, 5, 10, 50]$. The best-performing configuration was $k = 2, \gamma = 2, \kappa = 5$.

Table 6: Comparative evaluation on One-class. We report the mean of the AUA (\uparrow) over five trials. **Bold** and underlined indicate best and second best, respectively. Our method is among the two best methods for all cases.

	Plane	Car	Bird	Cat	Deer	Dog	Frog	Horse	Ship	Truck	Mean
SAL	61.8	83.3	59.1	62.1	64.7	65.3	74.2	68.9	76.1	86.0	70.2
HSC	82.6	81.0	64.7	<u>72</u>	71.5	70.7	82.0	78.7	87.2	86.0	77.6
ETLT	87.4	94.2	81.2	81.5	91.7	84.6	90.8	89.3	93.9	94.8	89.0
MahaAD	88.0	93.2	80.1	79.7	91.1	84.9	90.5	89.4	93.1	95.0	88.5
BCE	85.1	89.5	79.9	78.4	83.4	80.3	90.2	82.1	90.2	89.7	84.9
AdaODD	92.0	96.6	87.7	86.7	94.0	91.5	94.5	95.4	<u>95.5</u>	97.5	93.1
MDiff	93.0	94.3	<u>84.6</u>	81.3	92.2	88.4	93.8	91.1	95.1	95.8	91.0
ours	93.1	<u>95.5</u>	87.7	<u>84.9</u>	<u>93.2</u>	<u>90.7</u>	95.4	<u>95.1</u>	96.0	96.6	92.8

MDiff [47] models both the in- and out-distribution as a Gaussian and scores samples by the distance to the in-distribution minus the distance to the out-distribution. We use a multi-scale version with the pre-trained network using the same layers as MahaAD and our method. We search over the threshold τ used to pseudo-label incoming test samples. We search over $\tau \in [80, 85, 90, 95, 98]$. The best-performing configuration was $\tau = 85$.

Ours. We search over β , influencing the mixing of s^- and s^+ , in $\beta \in [100, 300, 500]$, and over γ , influencing the uncertainty scaling, in $\gamma \in [1, 3, 5]$, and the pseudo-labeling threshold $\tau \in [80, 90, 95]$. The best-performing configuration was $\beta = 100, \gamma = 5, \tau = 95$.

A.2 One-class AUA Results

We provide the AUA results on **One-class** in Tab. 6, which gives similar conclusions as the AUF in Tab. 2, except for AdaODD scoring comparatively better and BCE scoring comparatively worse. Our method performs well and is the only method to score in the top two for all ten experiments.